Available online at www.sciencedirect.com

SciVerse ScienceDirect

Ceramics International 39 (2013) 4713–4718

CERAMICS INTERNATIONAL

www.elsevier.com/locate/ceramint

Short communication

Microstructure–polarization relations in nickel/ gadolinia-doped ceria anode for intermediate-temperature solid oxide fuel cells

Yun-Gyeom Choi[a,b], Jun-Young Park[b], Huesup Song[c], Hae-Ryoung Kim[a], Ji-Won Son[a], Jong-Ho Lee[a], Hae-June Je[a], Byung-Kook Kim[a], Hae-Weon Lee[a], Kyung Joong Yoon[a,*]

[a]*High-Temperature Energy Materials Research Center, Korea Institute of Science and Technology, Seoul, Republic of Korea*
[b]*Nanotechnology and Advanced Materials Engineering, Sejong University, Seoul, Republic of Korea*
[c]*Division of Advanced Materials Engineering, Kongju National University, Chonan, Republic of Korea*

Received 9 August 2012; received in revised form 30 October 2012; accepted 7 November 2012
Available online 14 November 2012

Abstract

Intermediate-temperature solid oxide fuel cells (SOFCs) based on gadolinia-doped ceria (GDC) electrolyte were successfully fabricated. The cells were composed of Ni–GDC anode substrate, Ni–GDC anode functional layer, GDC electrolyte, $(La_{0.8}Sr_{0.2})CoO_3$ (LSC)–GDC cathode functional layer, and LSC cathode current collector. Anode substrates were fabricated by die compaction of granules prepared by spray drying process, and poly(methyl methacrylate) (PMMA) was employed as a pore former for rapid transport of reactant and product gases across the thick anode. The shape and the distribution of pores in the anode substrate were significantly affected by the properties of suspension in spray drying process, and a uniform and interconnected pore structure was obtained by increasing solids loading due to reduced phase separation. High solids loading also improved thermal compatibility between the anode and the electrolyte in a co-firing process, resulting in reduced micro-defects in the electrolyte. Substantial reduction of anode concentration polarization as well as increased open circuit voltage was measured in cell test, and the maximum power density of 550 mW cm^{-2} was obtained with humidified H_2 as fuel and air as oxidant at 650 °C.

Keywords: A. Suspensions; B. Porosity; D. CeO_2; E. Fuel Cells

1. Introduction

Gadolinia-doped ceria (GDC) has received increasing attention as an electrolyte material for intermediate-temperature solid oxide fuel cells (SOFCs) due to its high ionic conductivity, good chemical compatibility with cobalt-containing cathode materials, and close thermal expansion match with Ni-cermet anode and ferritic stainless steel interconnect [1]. In addition, Ni/GDC anode is known to possess superior catalytic activity toward fuel oxidation as well as improved carbon- and sulfur-tolerance compared to the conventional Ni/yttria-stabilized zirconia (YSZ) anode [2]. Therefore, anode-supported GDC-based cell could be a promising proposition for high performance intermediate-temperature SOFCs. In such cell configurations, the relatively thick anode substrate could contribute significantly to the performance loss due to concentration polarization caused by sluggish gas diffusion of reactants into and/or products out of the anode [3]. Since the pores produced by removal of oxygen from NiO during reduction are not sufficient to allow rapid gas transport, a pore former, which renders a porous structure after adequate thermal treatment, is necessary to generate additional porosity in the substrate. There are a number of pore former materials available for fabrication of the SOFC anode substrate, including graphite [4,5], carbon black [6,7], starch [5,8], polyamide [5] and poly(methyl methacrylate) (PMMA) [9–11]. It is known that the morphology of pores is closely related to the shape and size of the pore former [12], and PMMA microspheres could be a promising option

*Correspondence to: Korea Institute of Science and Technology, High-Temperature Energy Materials Research Center, Hwarangno 14-gil 5, Seongbuk-gu, Seoul 136-791, Korea. Tel.: +82 2 958 5515; fax: +82 2 958 5529.
E-mail address: kjyoon@kist.re.kr (K.J. Yoon).

0272-8842/$ - see front matter © 2012 Elsevier Ltd and Techna Group S.r.l. All rights reserved.
http://dx.doi.org/10.1016/j.ceramint.2012.11.020

to obtain optimum microstructure based on its geometry and purity [9,11]. However, PMMA often results in isolated and closed pores which hardly contribute to the gas transport [13,14]. Since the pore structure directly reflects the fabrication process, it is important to adopt adequate fabrication techniques and optimize the processing parameters to obtain interconnected pores for rapid gas transport and minimal concentration polarization.

Die compaction from powder granules is one of the simplest forms of consolidation process and offers numerous advantages for preparation of SOFC anode substrate, including high production rate, reproducibility, ease of automation, and absence of drying requirement [15]. For the compaction process, granulated feed materials with uniform and repeatable properties can be economically prepared using the spray drying technique, in which a fluid material is transformed into dry powder by spraying the feed into a hot drying medium [16]. Previously, we reported spray drying and compaction processes for cost-competitive fabrication of high performance YSZ-based SOFCs [17,18]. In the present study, the GDC-based anode-supported cells were successfully fabricated using the similar processing techniques. The effect of the suspension properties in spray drying process on the microstructural characteristics of the Ni/GDC anode substrate was investigated, and the process–microstructure–performance relationships are discussed in detail using the electrochemical test data.

2. Experimental

To prepare the slurry for spray drying, 10 mol% GDC, NiO, and PMMA were ball-milled for 24 h in ethanol with the desired amounts of binder (polyvinyl butyral), plasticizer (dibutyl phthalate), and polymeric surfactant (KD-6). Volume ratio of GDC, NiO, and PMMA was 0.37:0.33:0.3, and slurries with different solids loadings of 15 vol% and 25 vol% were used for granulation. The ceramic granules were obtained using a spray dryer equipped with an air pressured spraying nozzle at an inlet temperature of 120 °C, outlet temperature of 60 °C, and atomizing pressure of 0.3 kg cm^{-2}. Anode substrates (2 cm × 2 cm) were fabricated by uni-axially pressing the granules at 60 MPa. The anode functional layer slurry was prepared by milling NiO and GDC with solvent (α-terpineol), binder (EC-10), plasticizer (dibutyl phthalate), and dispersant (KD-1) in a desired ratio, and screen printed over the anode support. The electrolyte slurry was prepared by milling GDC with the same solvent and organic additives, and screen printed over the anode functional layer. The anode support, anode functional layer, and electrolyte were co-fired at 1430 °C. The anode functional layer was dense after the co-firing process, and became porous during operation due to loss of oxygen in reduction of NiO to metallic Ni. For preparation of cathode functional layer, $La_{0.8}Sr_{0.2}CoO_3$ (LSC) and GDC powders were mixed in a 1:1 weight ratio with the same solvent and organic additives, and screen printed over the electrolyte. The slurry for cathode current collector was prepared by milling GDC with the same solvent and organic additives, and screen printed over the cathode functional layer, followed by sintering at 950 °C in air. The effective electrode area was 1 cm × 1 cm. The fabricated cells were tested with humidified hydrogen (3% H_2O) as fuel and air as oxidant at 650 °C. Electrochemical measurements were performed using a Solartron 1260/1287 potentiostat and a frequency response analyzer. After testing, the cells were sectioned and impregnated with epoxy in vacuum. After the epoxy was hardened, they were polished down to 1 μm, and the cross-sections were examined using scanning electron microscopy (SEM) analysis (Philips FEI XL-30 FEG).

Sintering shrinkages of NiO/GDC compacts obtained from the suspensions with 15 vol% and 25 vol% solids loadings were measured using a dilatometer (Netzsch DIL 402C) up to 1450 °C in air with heating rate of 3 °C/min, and compared with that of GDC.

3. Results and discussion

Fig. 1(a) shows the cross-sectional SEM image of the fabricated cell. The cell is composed of ~900 μm-thick porous Ni–GDC anode support, ~10 μm-thick porous Ni–GDC anode functional layer, ~10 μm-thick dense GDC electrolyte, ~10 μm-thick porous LSC–GDC cathode functional layer, and ~10 μm-thick porous LSC cathode current collecting layer. The microstructures of the anode supports fabricated by compaction of granules, which were prepared by the spray drying process using suspensions with 15 vol% and 25 vol% solids loadings, are compared in Fig. 1(b) and (c), respectively. Through image analysis, both samples were found to have similar volume porosity (29–30%) because the compositions of the solids including the volume fraction of pore former were identical for both samples. However, pore structures are clearly different for the two samples. It is clearly seen that the anode substrate fabricated with low solids loadings (15 vol%) contains large amount of elongated pores and pore clusters (Fig. 1(b)), while high solids loadings in the spray drying process (25 vol%) results in uniformly distributed pores, maintaining the spherical shape of individual PMMA pore formers (Fig. 1(c)). In the image analysis, the average pore size was measured to be ~7.4 μm for Fig. 1(b) and ~5.7 μm for Fig. 1(c), and the average aspect ratio of pores was ~2.4 for Fig. 1(b) and ~1.3 for Fig. 1(c). In the spray drying process, the use of slurry with high solids loading is desirable for both economic and technical reasons. Economically, the capacity of the equipment is defined by the amount of solution that can be evaporated per unit time, and the output of granules increases with increasing the solids loading of the slurry for the fixed equipment capacity [19]. From the technical point of view, the granules obtained from the dilute suspension tend to be irregular and heterogeneous

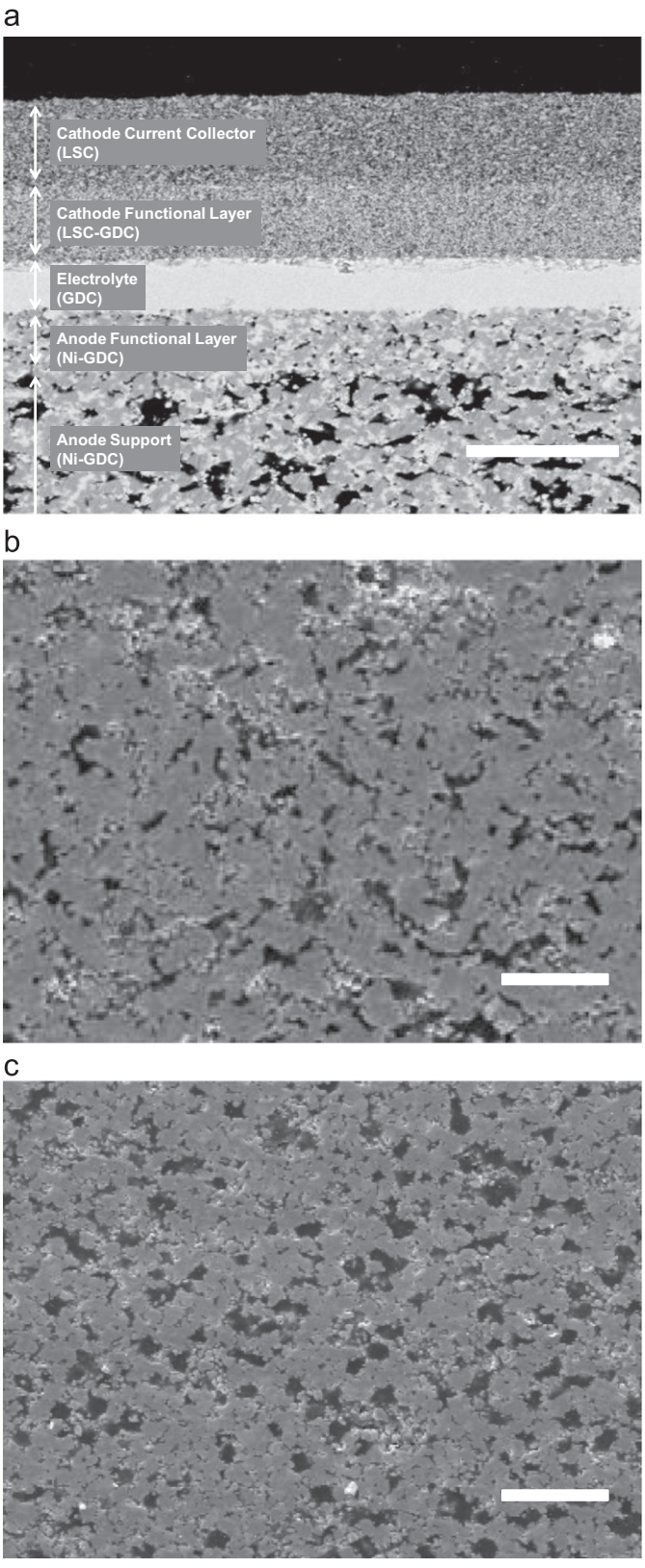

Fig. 1. SEM images of (a) cross-section of GDC-based cell, and anode substrate fabricated using suspension with (b) 15 vol%, and (c) 25 vol% solids loadings after reduction.

due to phase separation, resulting in poor packing and non-uniform microstructure of the final products [20]. Fig. 1(b) and (c) indicates that the properties of the suspension for spray drying process directly affect the morphology of the sintered anode substrate, and solids loading is a very important factor determining the size, shape and distribution of the pores. Uni-axial pressing often results in pore clusters aligned perpendicular to the compaction axis [21] as shown in Fig. 1(b), which could particularly be detrimental to gas transport because pores perpendicular to the gas flow lead to pressure drop and increase of pore tortuosity [21]. Fig. 1(c) shows that formation of such elongated pores and pore clusters can be suppressed in the compaction process by increasing the solids loading of the suspension and reducing the degree of phase separation in spray drying process.

The fabricated cells were electrochemically tested, and Fig. 2 shows the current density–voltage (I–V) characteristics and the corresponding power densities. The cells fabricated using the anode suspensions with 15 vol% and 25 vol% solids loadings will be denoted as cell-1 and cell-2, respectively. The maximum power densities were $\sim$300 mW cm^{-2} for cell-1 and $\sim$550 mW cm^{-2} for cell-2 at 650 °C. Performance and OCV of cell-2 were comparable to or slightly higher than the state-of-the-art cells with similar structure [2,22]. The I–V curve of cell-1 shows a convex-up curvature ($d^2V/dI^2 < 0$) at high current density above 1 A cm^{-2}, while cell-2 exhibits linear I–V relationship up to 2 A cm^{-2}. Because a convex-up curvature at high current density typically indicates concentration polarization [3], performance of cell-1 is considered to be limited by the gas diffusion of the reactant and/or product gases in the anode substrate at high current while gas transport across the anode substrate of cell-2 is sufficiently rapid to sustain such high current density. Open circuit voltages (OCVs) were 0.65 V for cell-1 and 0.74 V for cell-2 at 650 °C with humidified H_2 (3% H_2O) as fuel and air as oxidant. Reduction of the OCV from the theoretical Nernst potential is explained by the leakage electronic current through the electrolyte due to the mixed conducting nature of GDC in typical SOFC operating conditions [23].

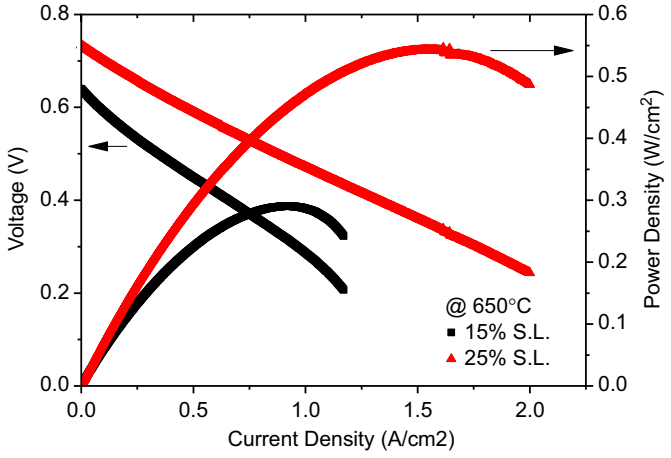

Fig. 2. I–V curves and power densities of the cells fabricated from 15 vol% and 25 vol% solids loadings measured with humidified hydrogen as fuel and air as oxidant at 650 °C.

The OCV of the cell-1 was lower than that of cell-2 by ~90 mV. The difference in OCVs might be due to the different GDC electrolyte thicknesses because the thickness of ceria electrolyte determines the magnitude of the leakage current, leading to low OCV with reduced electrolyte thickness [24]. However, SEM investigation in Fig. 3 revealed that the electrolyte thicknesses of the two cells were similar at 8–10 μm. In addition, macro-defects such as through-cracks were not observed in Fig. 3. In the literature, there is an inconsistency in OCV values for ceria-based electrolytes with similar thicknesses [25,26], which could possibly be explained by the variation in properties of the electrolyte film such as porosity, homogeneity, defects, etc. In general, GDC electrolyte is more sensitive to the microstructural heterogeneity than YSZ electrolyte because GDC exhibits inferior densification behavior and mechanical properties compared to YSZ [27]. In the co-firing process used in this study, the quality of the GDC electrolyte is significantly influenced by the thermal properties of NiO–GDC substrate because the film stress of the electrolyte is dependent upon the sintering shrinkage of the thick substrate [28]. Fig. 4 compares the linear sintering shrinkage of the GDC electrolyte with those of the anode substrates used for cell-1 (15 vol% solids loading) and cell-2 (25 vol.% solids loading). When PMMA is used as the pore former, it is important to suppress formation of processing defects in the electrolyte caused by thermal expansion of PMMA at the initial stage of thermal process [29]. The inset in Fig. 4 shows that the linear expansion of the green anode substrate is significantly smaller for cell-2 than for cell-1 up to ~250 °C, PMMA removal temperature. Therefore, it is suggested that formation of large PMMA clusters due to low solids loading results in significantly larger expansion of the anode substrate than that of the electrolyte, leading to tensile stress in the thin electrolyte layer in green state, which can eventually cause processing defects. Contrarily, defect formation in the electrolyte caused by expansion of PMMA at the initial stage of the thermal processing could be effectively prevented through uniform distribution of PMMA using suspension with high solids loading because thermal expansion of the anode substrate of cell-2 matches very well with that of GDC electrolyte below 250 °C in Fig. 4. At high temperatures, the substrate used for cell-1 exhibits smaller sintering shrinkage than that of the GDC electrolyte, resulting in tensile stress in the electrolyte layer throughout the entire sintering processes, which restrains sintering of the electrolyte and increases the possibility of defect formation such as microcracks [30]. On the other hand, the anode substrate used for cell-2 shrinks more than does the GDC electrolyte below 1050 °C and above 1400 °C. In these temperature ranges, the GDC electrolyte is under compressive stress which assists densification. Therefore, higher OCV of cell-2 could possibly be explained by reduced defect density and enhanced densification of GDC electrolyte due to better thermal compatibility with the substrate. Detailed analysis on the cell microstructure and processing defects will be reported in a separate paper.

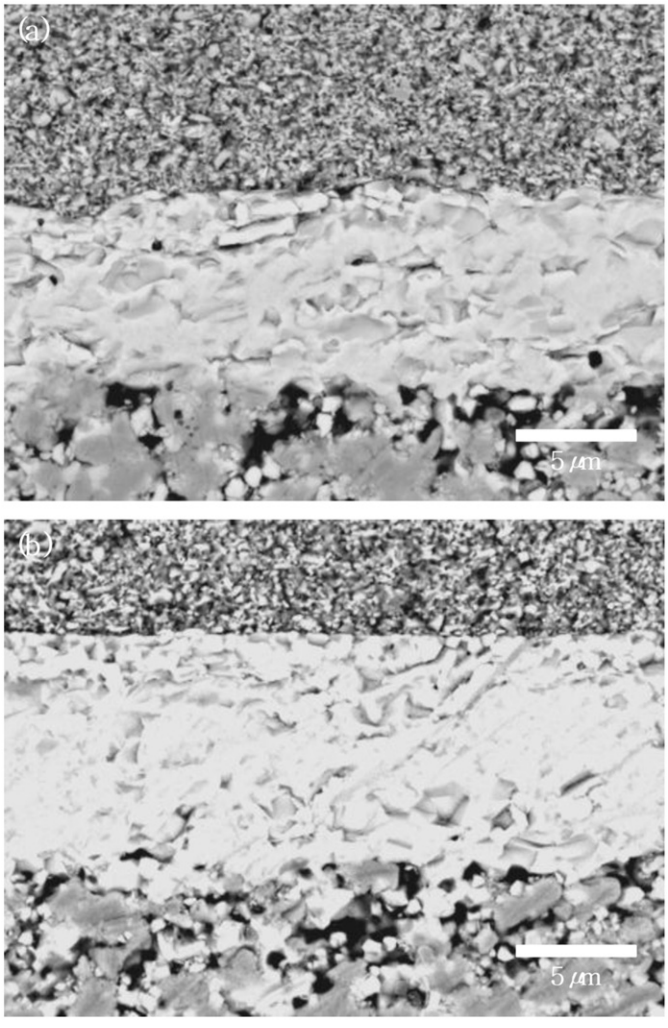

Fig. 3. SEM images of the GDC electrolyte fabricated using suspension with (b) 15 vol%, and (c) 25 vol% solids loadings after reduction.

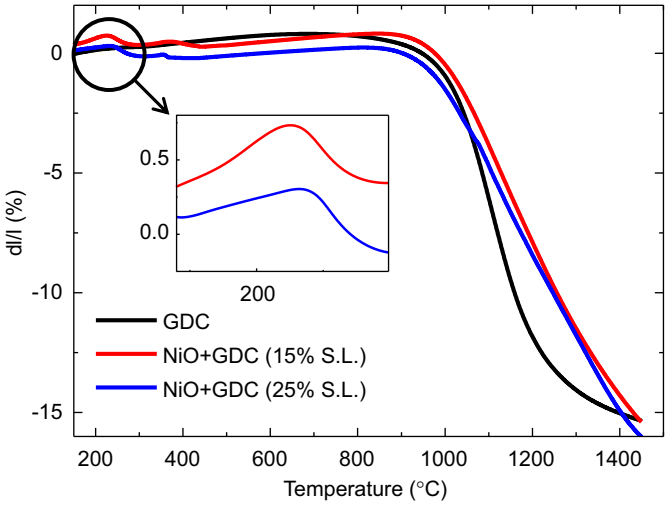

Fig. 4. Linear shrinkage of GDC electrolyte and NiO/GDC anode substrates fabricated from 15 vol% and 25 vol% solids loadings measured up to 1450 °C in air.

The cell polarization was investigated in detail using the impedance spectroscopy measured at 650°C in Fig. 5; cell-1 shows higher electrode polarization resistance (0.40 Ωcm^2) than does cell-2 (0.25 Ωcm^2) at OCV in Fig. 5(a). The ohmic resistance of cell-1 was slightly larger than that of the cell-2, but we believe that the difference is within the experimental error range. With dc-current of 1.2 A cm^{-2}, the impedance arc of cell-1 further expands to 0.54 Ωcm^2 while that of cell-2 shrinks to 0.15 Ωcm^2 in Fig. 5(b). In general, impedance spectra of SOFCs are composed of a number of overlapping depressed arcs reflecting physical and/or chemical processes associated with the electrode reaction [31], and each electrode process exhibits different response to the applied bias. The Bode plot in Fig. 5(c) shows the real and imaginary parts of impedance of cell-1 and cell-2 as a function of frequency at 1.2 A cm^{-2}, and difference between the two cells under applied bias is clearly observed in the low frequency range below 10 Hz. Decrease in polarization resistance of cell-2 with applied current in high frequency range ($> 10^2$ Hz) indicates that the electrode resistance is dominated by the surface exchange process [32] because the electrochemical reaction following the Butler–Volmer equation exhibits decreasing resistance with increasing dc-bias over the entire current range [33]. In case of cell-1, expansion of low frequency arc (< 10 Hz), which could be attributed to the gas diffusion in the anode substrate [34], is clearly visible with the same applied bias. This phenomenon could be explained by the limitation in gas transport across the anode substrate of cell-1 at high H_2 consumption and H_2O production rates associated with high operating current, and reflects the convex-up curvature at high current density in the *I–V* relationship observed in Fig. 2. Since the low frequency arc was not observed for cell-2 at the same current density, it is considered that the microstructure of the anode substrate is a critical factor determining the cell performance and the concentration polarization resistance can be significantly reduced by improving the pore distribution and connectivity.

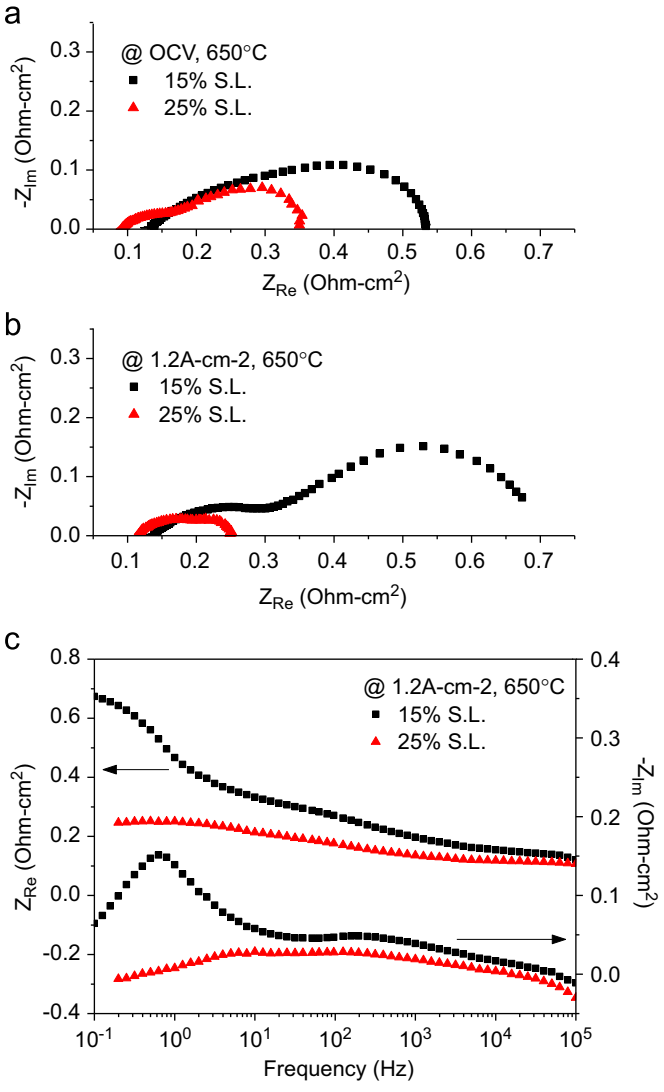

Fig. 5. Impedance spectra of the cells fabricated from 15 vol% and 25 vol % solids loadings. (a) Nyquist plot at OCV, (b) Nyquist plot at 1.2 A cm^{-2}, and (c) Bode plot at 1.2 A cm^{-2}.

4. Conclusion

GDC-based anode-supported SOFCs were successfully fabricated for intermediate-temperature operation. Spray drying and compaction processes are considered to be promising routes for economic production of Ni–GDC anode substrates, and the cell performance was strongly dependent on the microstructure of the substrate, which determines the mass transport of reactant and product gases during SOFC operation. Pore structure of the anode was tailored by engineering the properties of the suspension for spray drying process, which was directly reflected on the electrochemical performance. Further improvement is expected through the optimization of materials and processing parameters for GDC-based SOFCs.

Acknowledgment

This work was financially supported by the Institutional Research Program of Korea Institute of Science and Technology (2E22802) and the Seoul R&BD program (CS070157).

References

[1] S.C. Singhal, Advances in solid oxide fuel cell technology, Solid State Ionics 135 (1–4) (2000) 305–313.
[2] Y.D. Zhen, A.I.Y. Tok, S.P. Jiang, F.Y.C. Boey, Fabrication and performance of gadolinia-doped ceria-based intermediate-temperature solid oxide fuel cells, Journal of Power Sources 178 (1) (2008) 69–74.
[3] J.W. Kim, A.V. Virkar, K.Z. Fung, K. Mehta, S.C. Singhal, Polarization effects in intermediate temperature, anodesupported solid oxide fuel cells, Journal of the Electrochemical Society 146 (1) (1999) 69–78.
[4] K.B. Andersen, F.B. Nygaard, Z. He, M. Menon, K.K. Hansen, Optimizing the performance of porous electrochemical cells for flue gas purification using the DOE method, Ceramics International 37 (3) (2011) 903–911.

[5] Z. He, K. Andersen, L. Keel, F. Nygaard, M. Menon, K. Hansen, Processing and characterization of porous electrochemical cells for flue gas purification, Ionics 15 (4) (2009) 427–431.
[6] K.J. Yoon, P. Zink, S. Gopalan, U.B. Pal, Polarization measurements on single-step co-fired solid oxide fuel cells (SOFCs), Journal of Power Sources 172 (1) (2007) 39–49.
[7] F. Qiang, K. Sun, N. Zhang, S. Le, X. Zhu, J. Piao, Optimization on fabrication and performance of A-site-deficient $La_{0.58}Sr_{0.4}Co_{0.2}Fe_{0.8}O_3-\delta$ cathode for SOFC, Journal of Solid State Electrochemistry 13 (3) (2009) 455–467.
[8] C. Fu, X. Ge, S.H. Chan, Q. Liu, Fabrication and characterization of anode-supported low-temperature SOFC based on Gd-doped ceria electrolyte, Fuel Cells 12 (3) (2012) 450–456.
[9] B. Liang, T. Suzuki, K. Hamamoto, T. Yamaguchi, H. Sumi, Y. Fujishiro, et al., A reduced temperature solid oxide fuel cell with three-dimensionally ordered macroporous cathode, Journal of Power Sources 212 (0) (2012) 86–92.
[10] L. Mingyi, Y. Bo, X. Jingming, C. Jing, Influence of pore formers on physical properties and microstructures of supporting cathodes of solid oxide electrolysis cells, International Journal of Hydrogen Energy 35 (7) (2010) 2670–2674.
[11] M. Skovgaard, K.B. Andersen, K.K. Hansen, Pore former induced porosity in LSM/CGO cathodes for electrochemical cells for flue gas purification, Ceramics International 38 (2) (2012) 1751–1754.
[12] S.F. Corbin, J. Lee, X. Qiao, Influence of green formulation and pyrolyzable particulates on the porous microstructure and sintering characteristics of tape cast ceramics, Journal of the American Ceramic Society 84 (1) (2001) 41–47.
[13] M. Descamps, T. Duhoo, F. Monchau, J. Lu, P. Hardouin, J.C. Hornez, et al., Manufacture of macroporous β-tricalcium phosphate bioceramics, Journal of the European Ceramic Society 28 (1) (2008) 149–157.
[14] H. Santa Cruz, J. Spino, G. Grathwohl, Nanocrystalline ZrO2 ceramics with idealized macropores, Journal of the European Ceramic Society 28 (9) (2008) 1783–1791.
[15] K. Chen, X. Chen, Z. Lü, N. Ai, X. Huang, W. Su, Performance evolution of NiO/yttria-stabilized zirconia anodes fabricated at different compaction pressures, Electrochimica Acta 54 (4) (2009) 1355–1361.
[16] W.J. Walker Jr., J.S. Reed, S.K. Verma, Influence of slurry parameters on the characteristics of spray-dried granules, Journal of the American Ceramic Society 82 (7) (1999) 1711–1719.
[17] J.H. Lee, H. Moon, H.W. Lee, J. Kim, J.D. Kim, K.H. Yoon, Quantitative analysis of microstructure and its related electrical property of SOFC anode, Ni–YSZ cermet, Solid State Ionics 148 (1–2) (2002) 15–26.
[18] H.Y. Jung, S.H. Choi, H. Kim, J.W. Son, J. Kim, H.W. Lee, et al., Fabrication and performance evaluation of 3-cell SOFC stack based on planar 10 cm × 10 cm anode-supported cells, Journal of Power Sources 159 (1) (2006) 478–483.
[19] S.J. Lukasiewicz, Spray-drying ceramic powders, Journal of the American Ceramic Society 72 (4) (1989) 617–624.
[20] M. Vicent, E. Sánchez, A. Moreno, R. Moreno, Preparation of high solids content nano-titania suspensions to obtain spray-dried nanostructured powders for atmospheric plasma spraying, Journal of the European Ceramic Society 32 (1) (2012) 185–194.
[21] W.P. Pan, Z. Lü, K.F. Chen, Y.H. Zhang, B. Wei, Z.H. Wang, et al., Enhanced performance of solid oxide fuel cell by manipulating the orientation of cylindrical pores in anode substrate, Fuel Cells 12 (1) (2012) 41–46.
[22] S. Zha, W. Rauch, M. Liu, Ni–$Ce_{0.9}Gd_{0.1}O_{1.95}$ anode for GDC electrolyte-based low-temperature SOFCs, Solid State Ionics 166 (3–4) (2004) 241–250.
[23] S.M. Haile, Fuel cell materials and components, Acta Materialia 51 (19) (2003) 5981–6000.
[24] T. Matsui, T. Kosaka, M. Inaba, A. Mineshige, Z. Ogumi, Effects of mixed conduction on the open-circuit voltage of intermediate-temperature SOFCs based on Sm-doped ceria electrolytes, Solid State Ionics 176 (7–8) (2005) 663–668.
[25] D.J.L. Brett, A. Atkinson, N.P. Brandon, S.J. Skinner, Intermediate temperature solid oxide fuel cells, Chemical Society Reviews 37 (8) (2008) 1568–1578.
[26] B.C.H. Steele, Oxygen ion conductors and their technological applications, Materials Science and Engineering B 13 (2) (1992) 79–87.
[27] X. Zhang, C. Decès-Petit, S. Yick, M. Robertson, O. Kesler, R. Maric, et al., A study on sintering aids for $Sm_{0.2}Ce_{0.8}O_{1.9}$ electrolyte, Journal of Power Sources 162 (1) (2006) 480–485.
[28] M. Nagamori, T. Shimonosono, S. Sameshima, Y. Hirata, N. Matsunaga, Y. Sakka, Densification and cell performance of gadolinium-doped ceria (GDC) electrolyte/NiO–GDC anode laminates, Journal of the American Ceramic Society 92 (2009) S117–S121.
[29] D.S. Lee, J.H. Lee, J. Kim, H.W. Lee, H.S. Song, Tuning of the microstructure and electrical properties of SOFC anode via compaction pressure control during forming, Solid State Ionics 166 (1–2) (2004) 13–17.
[30] J.H. She, K. Ueno, Densification behavior and mechanical properties of pressureless-sintered silicon carbide ceramics with alumina and yttria additions, Materials Chemistry and Physics 59 (2) (1999) 139–142.
[31] S.H. Jensen, A. Hauch, P.V. Hendriksen, M. Mogensen, N. Bonanos, T. Jacobsen, A method to separate process contributions in impedance spectra by variation of test conditions, Journal of the Electrochemical Society 154 (12) (2007) B1325–B1330.
[32] E.J.L. Schouler, M. Kleitz, Electrocatalysis and inductive effects at the gas,Pt/stabilized zirconia interface, Journal of the Electrochemical Society 134 (5) (1987) 1045–1050.
[33] Z. Lu, J. Hardy, J. Templeton, J. Stevenson, New insights in the polarization resistance of anode-supported solid oxide fuel cells with $La_{0.6}Sr_{0.4}Co_{0.2}Fe_{0.8}O_3$ cathodes, Journal of Power Sources 196 (1) (2011) 39–45.
[34] R. Barfod, M. Mogensen, T. Klemenso, A. Hagen, Y.L. Liu, P.V. Hendriksen, Detailed characterization of anode-supported SOFCs by impedance spectroscopy, Journal of the Electrochemical Society 154 (4) (2007) B371–B378.